Lipid Headgroup Superlattice Modulates the Activity of Surface-Acting Cholesterol Oxidase in Ternary Phospholipid/Cholesterol Bilayers†

Kwan Hon Cheng,‡* Brian Cannon,‡ Jennifer Metze,‡ Anthony Lewis,‡ Juyang Huang,‡ Mark W. Vaughn,§ Qing Zhu,§ Pentti Somerharju,|| and Jorma Virtanen⊥

Departments of Physics and Chemical Engineering, Texas Tech University, Lubbock, Texas 79409, Institute of Biomedicine, University of Helsinki, Helsinki, Finland, and ⊥Department of Chemistry, NanoScience Center, University of Jyväskylä, Jyväskylä, Finland

Received May 11, 2006; Revised Manuscript Received June 21, 2006

ABSTRACT: The relationship between the molecular organization of lipid headgroups and the activity of surface-acting enzyme was examined using a bacterial cholesterol oxidase (COD) as a model. The initial rate of cholesterol oxidation by COD in fluid state 1-palmitoyl-2-oleoyl-phosphatidylethanolamine/1-palmitoyl-2-oleoyl-phosphatidylcholine/cholesterol (POPE/POPC/CHOL) bilayers was measured as a function of POPE-to-phospholipid mole ratio (X_{PE}) and cholesterol-to-lipid mole ratio (X_{CHOL}) at 37 °C. At $X_{PE} = 0$, the COD activity changed abruptly at $X_{CHOL} \approx 0.40$, whereas major activity peaks were detected at $X_{PE} \approx 0.18$, 0.32, 0.50, 0.64, and 0.73 when X_{CHOL} was fixed to 0.33 or 0.40. At a fixed X_{CHOL} of 0.50, the COD activity increased progressively with PE content and exhibited small peaks or kinks at $X_{PE} \approx 0.40$, 0.50, 0.58, 0.69, and 0.81. When X_{PE} and X_{CHOL} were systematically varied within a narrow 2-D lipid composition window, an onset of COD activity at $X_{CHOL} \approx 0.40$ and the elimination of the activity peak at $X_{PE} \approx 0.64$ for $X_{CHOL} > 0.40$ were clearly observed. Except for $X_{PE} \approx 0.40$ and 0.58, the observed critical PE mole ratios agree closely (±0.03) with those predicted by a headgroup superlattice model (Virtanen, J.A., et al. (1998) *Proc. Natl. Acad. Sci. U.S.A. 95,* 4964−4969; Cannon, B., et al. (2006) *J. Phys. Chem. B 110,* 6339−6350), which proposes that lipids with headgroups of different sizes tend to adopt regular, superlattice-like distributions at discrete and predictable compositions in fluid lipid bilayers. Our results indicate that headgroup superlattice domains exist in lipid bilayers and that they may play a crucial role in modulating the activity of enzymes acting on the cell membrane surface.

The lateral organization of phospholipid and cholesterol in cellular membranes and its effect on protein structure and function are thought to play a significant role in the pathogenesis and designing of therapeutic interventions for various diseases such as Alzheimer's, atherosclerosis, and bacterial or viral infections (*1*, *2*). For example, a membrane-surface-acting β-amyloid protein, a primary factor in Alzheimer's disease, has been shown to interact with membrane cholesterol (*3*−*5*). Cholesterol enriched lipid domains in the plasma membrane of vascular smooth muscle cells (SMC[1]) (*1*) appear to be linked to vascular diseases such as atherogenesis (*6*). In animal studies, amlodopine, a highly lipophilic and atheroprotective drug, has been shown to alter the abnormal cholesterol domains of SMC of the aorta, suggesting that cholesterol domains could be a potential therapeutic target when treating heart diseases (*7*). Cytolysins, a family of pore-forming toxins associated with bacteria, are known to rely on the membrane cholesterol of the targeted host cells for inserting their transmembrane complex to initiate cytolysis (*8*). Some bacteria also secrete a membrane-surface-acting enzyme, such as a cholesterol oxidase (COD), as part of a metabolic pathway to convert cholesterol to a carbon source and as a virulence factor to infect host cells through disruption of the host's membrane structures (*9*, *10*). At present, the detailed molecular organization of the phospholipid and cholesterol in membranes and its role in regulating the activity of the membrane-surface-acting enzyme are still unclear. Here, COD (EC 1.1.3.6) is selected as a model peptide to study the relationship between the phospholipid headgroup organization and membrane-surface-acting enzyme in a biologically relevant ternary lipid bilayer system.

COD is a water-soluble 56 kDa bacterial flavoenzyme. It acts on lipid membrane surfaces, where it catalyzes the conversion of cholesterol to cholest-3-en-4-one (*11*−*13*). The X-ray structure of COD has recently been reported (*12*). It is believed that COD exerts its initial action by first binding directly to the membrane surface without inducing major perturbations to the membrane structure (*14*). Upon mem-

† This work was supported by the Welch Research Foundation (D-1158) and the National Science Foundation (0344463 and 0134594).

* Corresponding author. Phone: 806-742-2992. Fax: 806-742-1182. E-mail: vckhc@ttacs.ttu.edu.

‡ Department of Physics, Texas Tech University.

§ Department of Chemical Engineering, Texas Tech University.

|| University of Helsinki.

⊥ University of Jyväskylä.

[1] Abbreviations: SMC, smooth muscle cells; COD, cholesterol oxidase, PL, phospholipid; CHOL, cholesterol; PE, phosphatidylethanolamine; PC, phosphatidylcholine; POPE, 1-palmitoyl-2-oleoyl-*sn*-glycero-3-PE; POPC, 1-palmitoyl-2-oleoyl-*sn*-glycero-3-PC; X_{PE}, POPE to PL mole ratio; X_{CHOL}, CHOL to total lipid mole ratio; RSE, rapid solvent exchange; LTT, low temperature trapping; POD, peroxidase; MD, molecular dynamics; pdb, protein data bank.

10.1021/bi060937y CCC: $33.50
Published on Web 08/16/2006

brane binding, COD undergoes a conformational change, which leads to the formation of a hydrophobic channel allowing the access of cholesterol to the active site of the enzyme (*11*, *15*, *16*). The activity of COD is sensitive to the physiochemical and biophysical properties of the membranes, such as bulk lipid compositions (e.g., phospholipid (PL), headgroup composition, and cholesterol concentration) and lipid packing order or phase state, that is, solid versus fluid, in cholesterol containing lipid membranes (*16*−*19*).

Recent studies have indicated that the activity of COD is markedly modulated by membrane cholesterol (CHOL) content and its lateral distribution behavior (*20*−*22*). These studies were carried out largely with binary PL/CHOL bilayers. However, these studies did not clarify the role of the PL headgroup organization on lipid membrane surface. Furthermore, biological membranes are more complex than binary lipid bilayers. In this study, the three lipids, phosphatidylethanolamine (PE), phosphatidylcholine (PC), and CHOL, represent the major lipid components of most mammalian cell plasma membranes. Therefore, the results obtained from the pure PE/PC/CHOL ternary bilayers are relevant to reveal the subtle regulation mechanisms of membrane lipid composition and surface molecular structures on the membrane-surface-acting enzyme in cell membranes.

In the present study, we have systematically studied the activity of COD on ternary bilayers consisting of 1-palmitoyl-2-oleoyl-PE (POPE), 1-palmitoyl-2-oleoyl-PC (POPC), and cholesterol. We did this by varying the amount of POPE-to-total PL mole ratio (X_{PE}) and the cholesterol-to-total lipid mole ratio (X_{CHOL}). Prominent peaks in COD activity were found at certain X_{PE} values at a fixed X_{CHOL}. Most of these X_{PE} values coincide closely with the critical X_{PE} values predicted by the lipid headgroup superlattice model (*23*−*26*). This headgroup superlattice model suggests that the phospholipids of different headgroup sizes, that is, PE and PC, can form regular or superlattice-like arrangements or domains in fluid state lipid membranes (*24*, *25*). The presence of headgroup superlattice domains was recently implicated by steady-state and time-resolved fluorescence spectroscopy and noninvasive Fourier transform IR spectroscopy in both binary POPE/POPC (*23*, *27*) and ternary POPE/POPC/CHOL (*26*) lipid bilayers. In this study, using molecular dynamics simulations, the steric feasibility of headgroup superlattice structure in the presence of cholesterol was also demonstrated at the atomic level. Our results provide independent evidence that these headgroup superlattice domains exist in the ternary lipid bilayer and, importantly, that these headgroup superlattice domains strongly affect or modulate the activity of COD and, perhaps, that of other membrane-surface-acting enzymes in cell membranes.

MATERIALS AND METHODS

Materials. POPE and POPC were purchased from Avanti Polar Lipids, Inc. (Alabaster, AL) and cholesterol from Nu Chek Prep, Inc. (Elysian, MN). Lipid purity (>99%) was confirmed by thin layer chromatography on washed, activated silica gel plates (Alltech Associates, Inc., Deerfield, IL) and developed with chloroform/methanol/water = 65:25:4 for phospholipid analysis or with petroleum ether/ethyl ether/chloroform = 7:3:3 for cholesterol analysis. All solvents were of HPLC grade. The concentrations of all phospholipid stock solutions were determined by a phosphate assay (*28*). Aqueous buffer (pH 7.0, 5mM PIPES, 200mM KCl, 1 mM EDTA, 1 mM NaN_3) was prepared from deionized water (~18 MΩ) and filtered through a 0.1 μm filter before use. Recombinant COD expressed in *E. coli* (C-1235), peroxidase (P-8250) from horseradish, and other chemicals for the cholesterol oxidation measurements were purchased from Sigma (St. Louis, MO).

Liposome Preparation. Three liposome preparation methods, extrusion (*29*), ethanol injection (*30*), and rapid solvent exchange (*31*), were used for the cholesterol oxidation experiments. For the extrusion method, multilamellar liposomes were prepared using a low-temperature trapping (LTT) technique (*32*, *33*). LTT produces homogeneous and compositionally uniform liposomes even at high cholesterol contents, which is particularly important in the present context. In order to reduce the size of the liposomes, the liposomes prepared by LTT were repeatedly extruded through a double-stacked 0.1 μm pore size polycarbonate filters at a pressure of 200 PSI using an extruder (Lipex Biomembranes Inc., Vancouver, British Colombia, Canada). Afterward, the total phospholipid and cholesterol concentrations were checked following extrusion with phosphate (*28*) and cholesterol (*34*) assays. For the ethanol injection method, the lipids were mixed in chloroform. The chloroform was then removed under a vacuum of 30 mTorr for 12 h. The dried lipids were then dissolved in 25 μL of dry ethanol. The ethanol-dissolved lipids were then slowly added to a vortexing aqueous PBS buffer (800 μL), preheated to 45 °C, and liposomes were subsequently formed. For the rapid solvent exchange (RSE) method (*31*), the lipids were first dissolved in 100 μL of chloroform. The lipid solution was then heated to 50 °C in a glass tube and an aqueous PIPES buffer (800 μL) was added. While keeping the mixture vigorously vortexing in the glass tube, the pressure inside the tube was gradually reduced to about 4 cm of Hg using a home-built vacuum attachment. After an additional minute of vortexing to remove the trace chloroform, RSE-liposomes were formed. Liposomes prepared by each of the above procedures were sealed under argon and stored at 23 °C on a mechanical shaker for at least 6 days before oxidation measurements. The samples were usually vortexed vigorously once a day during this equilibration period to prevent aggregation.

Cholesterol Oxidation Measurements. The initial oxidation rate of cholesterol by the COD enzyme was determined spectrophotometrically through the coupled-enzyme assay scheme as shown below. The total reaction involves two steps. In the first step, the COD-mediated oxidation of membrane cholesterol produces two products, hydrogen peroxide and cholest-3-en-4-one. Catalyzed by peroxidase (POD), the production of hydrogen peroxide in the first step subsequently reacts with 4-aminoantipyrine and phenol and produces red colored quinoneimine, which has a distinctive absorption peak at 500 nm (*34*). The rate-limiting step in this reaction is the slow reaction rate of COD with the membrane cholesterol.

$$\text{Cholesterol} + O_2 \xrightarrow{\text{COD}} H_2O_2 + \text{Cholest-4-en-3-one}$$

$$2H_2O_2 + \text{4-Aminoantipyrine} + \text{Phenol} \xrightarrow{\text{POD}} \text{Red Quinoneimine} + H_2O$$

For each cholesterol oxidation measurement, 0.8 mL of liposomes was first mixed with a 0.2 mL solution containing 140 mM phenol. After mixing, 1 mL of reaction buffer (1.64 mM aminoantipyrene and 10 000 U/L of peroxidase in PBS buffer at pH 7.40) was added. The above mixture was then incubated at 37 °C for at least 20 min and finally transferred to a cuvette. The sample in the cuvette was maintained at 37 °C and stirred with a mini stir bar during the measurement. An HP-8453 (UV/vis) linear diode array spectrophotometer (Agilent Technologies, Wilmington, DE) equipped with a multicell transport was used to measure the time-resolved UV/vis absorption spectra of the samples. The reaction was started by adding 20 μL of COD solution (0.02 U/mL) into the cuvette. The time-resolved UV/vis absorption spectra (300−900 nm) were collected with an accumulation time of 2 s per spectrum and a resolution of 2 nm per spectrum. Depending on the samples, the acquisition parameters for this study were as follows: time interval between two consecutive spectra = 35−120 s and total data collection time per sample = 20−60 min. Background-corrected time-dependent absorbance of quinoneimine was determined by calculating the difference of the absorbance at 500 nm and the background at 800 nm as a function of time. The initial oxidation rate defined by the rate of change in the quinoneimine absorbance at time zero was determined from a second-order polynomial fit to the absorbance data for the first 500 or 1000 s. All data acquisition and data analyses were performed using the UV−visible ChemStation Software provided by Agilent Technologies. For all experiments, regardless of the variable PE and CHOL mole ratios, the activity of COD was determined from samples with a fixed number of moles of cholesterol, ensuring that the bulk concentration of available substrate to COD remained constant from one sample to the other.

Lipid Superlattice Theory. The model proposes that phospholipids with different molecular structures, such as the PE and PC used in this study, tend to form hexagonal (HX), centered rectangular (CR), or rectangular (R) superlattice-like or regular distributions at the PL headgroup level (*23*, *24*, *27*). The molecular structures of POPC and POPE used in this study are shown in Figure 1. Note that the acyl chain compositions of POPC and POPE are identical, ensuring that the molecular organization of the two PLs is mainly due to the structural difference of the headgroups. This model further predicts that abrupt changes in bilayer properties may occur at certain discrete and predictable critical compositions. Those theoretical compositions can be derived from simple geometrical or symmetry principles (*24*). In our case, the critical PE mole fraction (PE/(PE + PC)), that is, X^{HX}_{HG}, X^{CR}_{HG}, or X^{R}_{HG}, for a superlattice headgroup structure with HX, CR, or R symmetry, respectively, is given by $1/((a^2 + ab + b^2))$, $1/(2ab + b^2)$, or $1/((ab + b^2)/2)$, respectively, for $X_{PE} < 0.5$ (*26*). Here PE is the guest and PC the host lattice component within the superlattice structure. However, when $X_{PE} > 0.5$, the roles of PE and PC are reversed, and PE becomes the host and PC the guest. The corresponding critical fraction is $1 - 1/((a^2+ab+b^2))$, $1 - 1/(2ab+b^2)$, or $1 - 1/((ab+b^2)/2)$, respectively, (*26*). In the above equations, *a* and *b* are lattice coordinates describing the distance between two proximal guest elements in lattice sites along the molecular or principal lattice axes (*26*). Each headgroup superlattice is therefore uniquely identified by lattice coordinates (*a*, *b*). A list of the predicted headgroup superlattices is shown in Table 1, and detailed descriptions of the headgroup superlattice model can be found elsewhere (*23*, *24*, *26*). Other than the headgroup superlattice, cholesterol can also exhibit regular or superlattice-like distribution at the tail group level of the lipid bilayer (*25*, *35*, *36*). The predicted critical cholesterol mole fractions for $X_{CHOL} \geq 0.20$ are 0.200, 0.220, 0.250, 0.286, 0.333, 0.400, 0.500, and 0.667 (*36*, *37*).

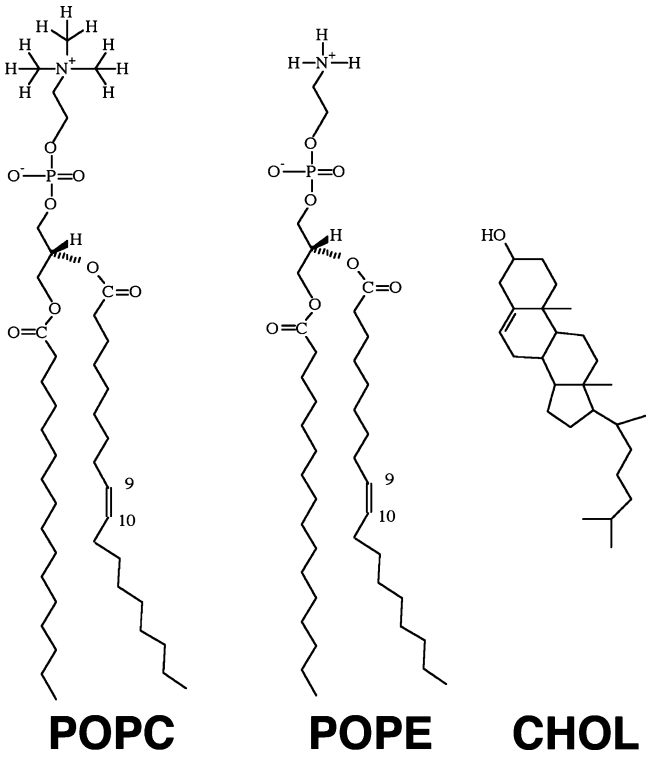

FIGURE 1: Molecular structures of POPC, POPE, and Cholesterol.

Visualization of the Molecular Organization of Superlattice Structures. To visualize the steric feasibility of the molecular components within the superlattice with atomic detail, 3-D molecular modeling and the molecular dynamics (MD) simulation of a hydrated ternary bilayer of POPE/POPC/CHOL at the superlattice compositions of $X_{CHOL} = 0.40$ (*26*, *35*, *36*) and $X_{PE} = 0.67$ (*23*−*25*) were performed using home-written software and GROMACS 3.3, a MD simulation and analysis package (*38*−*40*), respectively. The basic rule of building the 3-D superlattice geometry of the POPE/POPC/CHOL bilayer at $X_{CHOL} = 0.40$ and $X_{PE} = 0.67$ is that the center-of-mass position for each lipid had to agree with the lateral arrangement of the cholesterol (tail-group) and phospholipid headgroup according to a recently proposed simultaneous tail-group and headgroup superlattice structures in a 2-D space-filling model of identical lipid compositions (*26*). Published molecular coordinate files for POPC (*41*, *42*), POPE (*42*, *43*), and CHOL (*38*, *44*) in protein data bank (pdb) format (*45*) were collected. The structures of POPC and POPE were compacted and energy minimized using Hyperchem (Hypercube, Inc. Gainesville, FL). An initial 3-D ternary bilayer structure was subsequently created by using a home-written software, which allowed us to translate and rotate the individual lipid coordinates to precisely match the desired center-of-mass locations prescribed by the simultaneous tail-group and headgroup superlattice structures (*26*).

Table 1: Comparison of Critical Mole Fractions X_{PE} from COD Activity Measurements with X^{HX}_{HG}, X^{CR}_{HG}, or X^{R}_{HG} Values Predicted by the Headgroup Superlattice Model for Ternary Mixtures of POPE/POPC/Cholesterol at a Fixed Cholesterol/Lipid Ratio of $X_{CHOL} = 0.33$, 0.40, 0.44, and 0.50[a]

X^{HX}_{HG}, X^{CR}_{HG}, or X^{R}_{HG}	$X_{CHOL} = 0.33$	$X_{CHOL} = 0.40$	$X_{CHOL} = 0.44$	$X_{CHOL} = 0.50$
$0.11-0.13^{H,CR,R}$				
$0.14^{H,CR}$, 0.17^{R}	0.17		0.16	
0.20^{CR}		0.19		
$0.25^{H,CR,R}$				
$0.33^{H,CR}$	0.33	0.30	0.32	
		0.39[b]	0.41[b]	0.40[b]
0.50^{R}	0.53	0.47		0.50
				0.58[b]
$0.67^{H,CR}$	0.65	0.64	0.64	0.69
$0.75^{H,CR}$	0.74	0.72		
0.80^{CR}				0.81
0.83^{R}, $0.86^{H,CR}$				
$0.87-0.89^{R,CR,H}$				

[a] The critical mole fractions are identified from the peaks of the two-pass-2-point running averages of the raw data (see Results). Superscripts H, CR, and R denote X^{HX}_{HG}, X^{CR}_{HG}, or X^{R}_{HG}, respectively, from the headgroup superlattice model (see Materials and Methods). [b] Critical mole fractions that do not agree (±0.03) with X^{HX}_{HG}, X^{CR}_{HG}, or X^{R}_{HG} values.

No overlaps of atoms of any lipid from adjacent lipids were allowed. The final preassembled bilayer consisted of 48 POPC, 96 POPE, 96 cholesterol, and 6885 water molecules in a $6.7 \times 7.9 \times 7.8$ nm^3 initial system size. This bilayer was then compressed and energy minimized using GROMACS (*38*−*40*). A modest 30 ns MD simulation was performed (*46*−*52*). The details of force field parameters among lipids, that is, electrostatic (*49*, *50*) and van der Waals (*38*) interactions and bond length constraints (*51*), are given elsewhere. The 3-D structures of the ternary bilayer were visualized using an interactive molecular graphics software, Visual Molecular Dynamics, VMD 1.8.4b11 (*53*).

RESULTS

Cholesterol Oxidation Measurements in Control Binary POPC/CHOL Bilayers. The initial rate of oxidation of membrane cholesterol by the membrane-surface-acting enzyme COD was measured using a coupled-enzyme system as described in Materials and Methods. Figure 2 shows the representative time-resolved UV/vis absorption spectral measurements for POPC/CHOL binary mixtures at X_{CHOL} values of 0.32, 0.40, or 0.48 for liposomes prepared by the ethanol injection method, and the total cholesterol concentration in each sample was fixed at 130 μM. Note that this binary system serves as a control, that is, with $X_{PE} = 0$, for ternary POPE/POPC/CHOL mixtures. Clearly, the rate of cholesterol oxidation depended strongly on its mole fraction being slowest at $X_{CHOL} = 0.32$ (Figure 2A) and the highest at $X_{CHOL} = 0.48$ (Figure 2C). Because the total cholesterol substrate concentration was fixed (see Materials and Methods), the differences in the measured oxidation rate are related to differences in X_{CHOL}, that is, cholesterol surface density, in the bilayers. The initial rates in the representative assays were found to be 0.24, 2.6, and 11.9×10^{-4} s^{-1} for $X_{CHOL} = 0.32$, 0.40, and 0.48, respectively, as shown in Figure 2D. Therefore, the cholesterol oxidation rate for $X_{CHOL} = 0.48$ was approximately 6- or 50-fold greater than that for $X_{CHOL} = 0.40$ or 0.32, respectively.

Figure 3 shows the COD activity as a function of X_{CHOL} for POPC/CHOL liposomes. A clear onset, or an abrupt increase, of COD activity was observed at $X_{CHOL} \approx 0.40$.

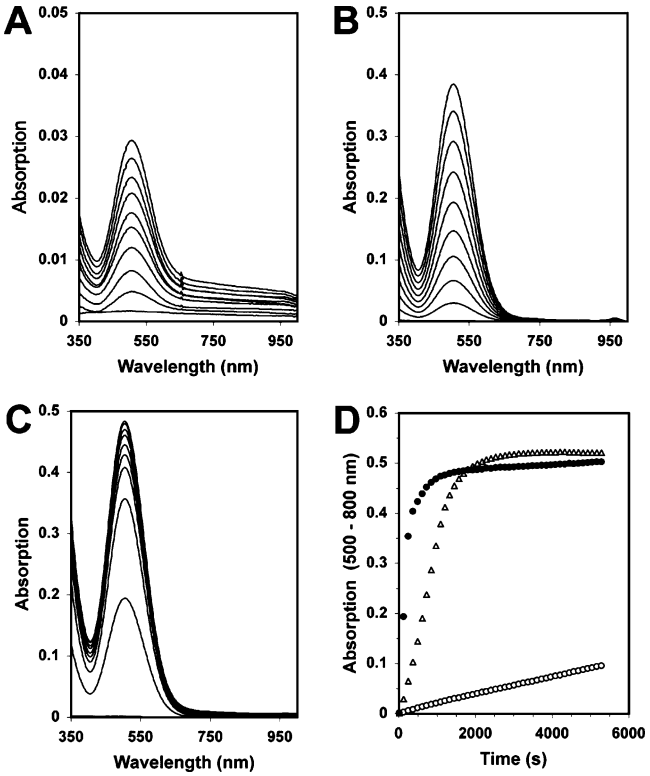

FIGURE 2: Representative COD activity assays on POPC/CHOL liposomes. The absorption spectra of quinoneimine, the final couple enzyme reaction product for POPC/CHOL liposomes prepared by the ethanol injection method (See Materials and Methods) as a function of time at 37 °C for cholesterol-to-lipid mole fraction (X_{CHOL}) = 0.32 (A), 0.40 (B), or 0.48 (C) are shown. The samples were kept in the dark for 6 days before the measurements. The main absorption band of quinoneimine with a peak centered at 500 nm is evident in all of the time-dependent spectra, as shown in panel A. For clarity, only the first 12 time-resolved absorption spectra, with an acquisition time of 2 s per spectrum and the time interval of 120 s separating two consecutive spectra for each X_{CHOL} are shown in this demonstration. The background corrected absorbance value of quinoneimine, i.e., absorbance at 500 nm minus absorbance at 800 nm ($A_{500} - A_{800}$), was calculated as a function of time. The plot of this corrected absorbance ($A_{500} - A_{800}$) as a function of time (panel D) for $X_{CHOL} = 0.32$ (○), 0.40 (△) and 0.48 (●) are shown. The total cholesterol concentration in each sample was fixed to 130 μM.

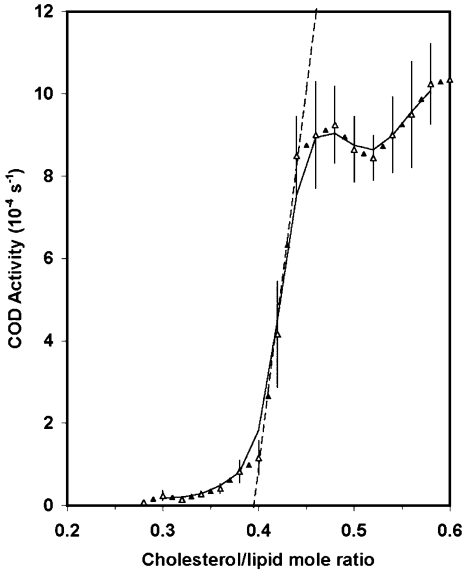

FIGURE 3: COD activity as a function of cholesterol-to-lipid mole ratio for POPC/CHOL liposomes. The COD activity as a function of cholesterol-to-lipid mole ratio for POPC/CHOL liposomes at 37 °C is shown. The data (○) represent averages from measurements of six parallel and independently prepared liposome preparations with bars indicate standard errors of measurements. The one- (▲) and two- (—) pass 2-point running averages (*32*) are also shown. The dotted line represents the extrapolation of the linear region of the activities beyond the onset of COD activities.

This onset was determined by extrapolating the linear region of the COD activity to the composition axis in the plot, as shown in Figure 3. Another, less pronounced onset was also evident at $X_{CHOL} \approx 0.50$. The above onset behavior was observed in identical COD activity measurements with liposomes prepared by other liposome preparation methods, that is, extrusion and RSE (see Materials and Methods).

Cholesterol Oxidation Measurements in Ternary POPE/POPC/CHOL Bilayers. COD activities for ternary POPE/POPC/CHOL liposomes with different X_{PE} and X_{CHOL} contents were performed. The liposomes were prepared by the RSE method (see Materials and Methods). The rationale for using the RSE method here instead of the ethanol injection method is described in the Discussion section below. The total cholesterol concentration of each sample was fixed at 40 μM. Figure 4 shows COD activity as a function of X_{PE} for a fixed X_{CHOL} value of 0.33, 0.40, 0.44, or 0.50. For $X_{CHOL} \leq 0.44$ (Figure 4 A−C), the overall level of COD activity was within the range of $0.5-3 \times 10^{-4}$ s^{-1}, and peaks of activity were evident at certain critical PE contents. However, at $X_{CHOL} = 0.50$ (Figure 4D), the shape of the COD activity plot changed drastically, and the peaks at $X_{CHOL} \leq 0.44$ were now replaced by small peaks or kinks at $X_{CHOL} = 0.50$. Other than a drastic change in the shape, the activity profile of COD was in the range of $2-35 \times 10^{-4}$ s^{-1} and greatly exceeded the $0.5-3 \times 10^{-4}$ s^{-1} level observed at lower cholesterol contents (Figure 4 A−C). These results suggest an existence of an onset or threshold of COD activity at $X_{CHOL} \approx 0.40-0.44$. This onset appears to become more prominent with increasing PE content.

To better determine the locations of the COD activity peaks or kinks, one- and two-pass 2-point running average protocols were employed (*32*) as shown in Figures 3 and 4. Such a multipass data smoothing protocol (*54*) suppresses data scatter due to uncertainties in data collection and sample preparation. Because of the use of multipoint running averages, the peaks or kinks defined by two or more primary data points were considered significant (cf. Figures 3 and 4). Table 1 lists the locations of the COD activity peaks and kinks along with the critical mole fractions predicted by the headgroup superlattice model for the superlattice structure with HX, CR, or R symmetry (see Materials and Methods).

To further explore the dependence of COD activities with PE and cholesterol contents, liposomes with PE and cholesterol mole fractions, systematically varying within a narrow 2-D lipid composition window ($X_{PE} = 0.58$ to 0.72; $X_{CHOL} = 0.34$ to 0.48), were examined. A composition increment of 0.02 was set for either PE or cholesterol mole fraction. The selected PE composition range covered the prominent activity peak at $X_{PE} \approx 0.64$, whereas the cholesterol composition range included the onset of COD activity at $X_{CHOL} \approx 0.4-0.44$, as shown in Figure 4. Representative plots of COD activity versus X_{PE} or X_{CHOL} values are shown in Figure 5. When X_{PE} was varied at a fixed X_{CHOL} (Figure 5A), a COD activity peak was evident at $X_{PE} \approx 0.65$ for $X_{CHOL} = 0.34$ and 0.40, in agreement with the results shown in Figure 4. However, when X_{CHOL} reached 0.46, the activity peak was replaced by a kink at a similar location, as shown in Figure 5A. When X_{CHOL} was varied at fixed X_{PE} (Figure 5B), an onset of COD activity at $X_{CHOL} \approx 0.40-0.44$ was evident for $X_{PE} = 0.58$, 0.64, and 0.72. Interestingly, the sharpness of onset appears to increase with increasing X_{PE} values.

Figure 6 shows the 3-D surface plot of COD activity as a function of X_{PE} and X_{CHOL}. The data points were normalized with respect to the activity at (X_{PE}, X_{PE}) = (0.72, 0.48). The overall shape of the 3-D surface indicates that COD activity increased progressively with increasing X_{PE} and X_{CHOL} values and reached a maximum at X_{PE}, $X_{CHOL} = 0.72$, 0.48. A small, local maximum was found at X_{PE}, $X_{PE} \approx 0.64-0.68$, 0.34−0.40. In addition, the rise of COD activity along the X_{CHOL} axis became steeper with increasing X_{PE} values (Figure 6). These 3-D data agree with the above 2-D plots (Figures 4 and 5) in that the activity peak of $X_{PE} \approx 0.64$ at high cholesterol content is eliminated, and the sharpness of onset at $X_{CHOL} \approx 0.40-0.44$ increased at high X_{PE}.

Visualization of the Surface Molecular Organization of Ternary POPE/POPC/CHOL Bilayers. Because COD interacts only with the lipid bilayer surface, it is useful to visualize the molecular arrangements of the polar groups of lipids on the bilayer surface. In addition, the steric feasibility of the components of lipids within the proposed simultaneous tail-group and phospholipid headgroup superlattice structures had to be established at the molecular level. MD simulation provided a useful tool to visualize the surface molecular organization of our proposed superlattice structures. On the basis of the recently published 2-D single-point space-filling constructions of simultaneous tail-group and headgroup superlattice structures (*26*), molecular assembling and a subsequent 30 ns MD simulation were performed (see Materials and Methods). Figure 7A shows the possible molecular organization of the each lipid, POPC (two orange disks), POPE (two blue disks joined by a bar), or CHOL (single yellow disk), at the lipid tail group level according to the single-point space-filling construction method at the

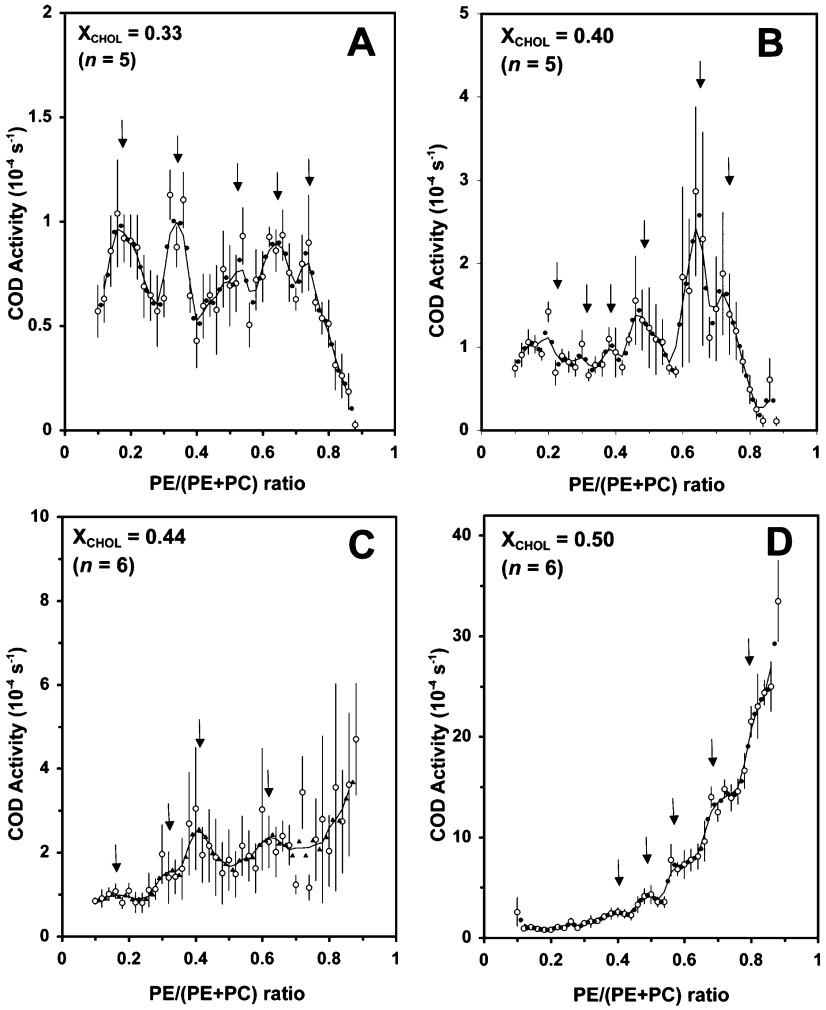

FIGURE 4: COD activity as a function of PE-to-(PE + PC) mole ratio for POPE/POPC/CHOL liposomes. The COD activity as a function of PE/(PE + PC) mole ratio for POPE/POPC/CHOL liposomes at 37 °C for a fixed cholesterol-to-lipid ratio (X_{CHOL}) of 0.33 (A), 0.40 (B), 0.44 (C), and 0.50 (B) is shown. The total cholesterol concentration was 40 μM. The arrows indicate the activity peaks as determined by the two-pass 2-point running averages (see Results). The data represent averages of measurements from five or six parallel and independently prepared liposome preparations. See the legend of Figure 3 for other details.

critical compositions of $X_{PE} = 0.67$ and $X_{CHOL} = 0.40$ (*26*). Note that both the PL headgroup and cholesterol exhibit a superlattice arrangement with CR symmetry, and their repeating unit cells are also identified. Figure 7B shows the successful 30 ns molecular dynamics simulated organization of the bilayer surface. For clarity, only the polar headgroup of each PL and the 3-β polar group of cholesterol are shown using VMD 1.8.4b11 (see Materials and Methods). Similar color representations in both the 2-D space-filling construction (Figure 7A) and the 3-D molecular visualization of the surface structure (Figure 7B) were used to facilitate the visual comparison of the lateral organization of the lipids. The superlattice-like distribution of cholesterol as well as the PL headgroup appears to be preserved on the membrane surface. During the modest 30 ns simulation, some rotation and translation of the lipids, especially cholesterol and the PE, which has a smaller headgroup compared with that of PC (Figure 1), were evident. All lipids remained in bilayer form throughout the simulation period. Longer simulations, the stability of superlattice geometry, and an extensive analysis of this ternary bilayer using MD will be presented in future studies.

DISCUSSION

The role of molecular organization of lipid components in the form of rafts or nanoscale domains in modulating cell membrane activities has been a subject of extensive interests (*1*, *2*, *55*−*58*). Cholesterol has been identified as the key component in those rafts or domains (*1*, *56*). The role of membrane cholesterol content and its lateral organization in regulating the activity of membrane-surface-acting enzymes has been studied extensively in several lipid bilayer and cell membrane systems (*16*, *18*, *22*, *59*). For example, Wang et al. (*22*) found discrete peaks in COD activity at X_{CHOL} values of 0.20, 0.25, and 0.33 for binary PC/cholesterol bilayers. These critical X_{CHOL} values agree with those predicted by the cholesterol superlattice model (*25*, *35*, *36*), which proposes that cholesterol and the acyl chains of PL tend to adopt regular superlattice-like distributions at the acyl chain level of lipid bilayers, and this lateral organization of cholesterol regulates the activity of the surface-acting enzyme. This study focused on the role of PL headgroup lateral organization on the activity of COD at fixed cholesterol content.

In the present study, we found that oxidation of cholesterol in ternary POPE/POPC/CHOL bilayers by COD shows

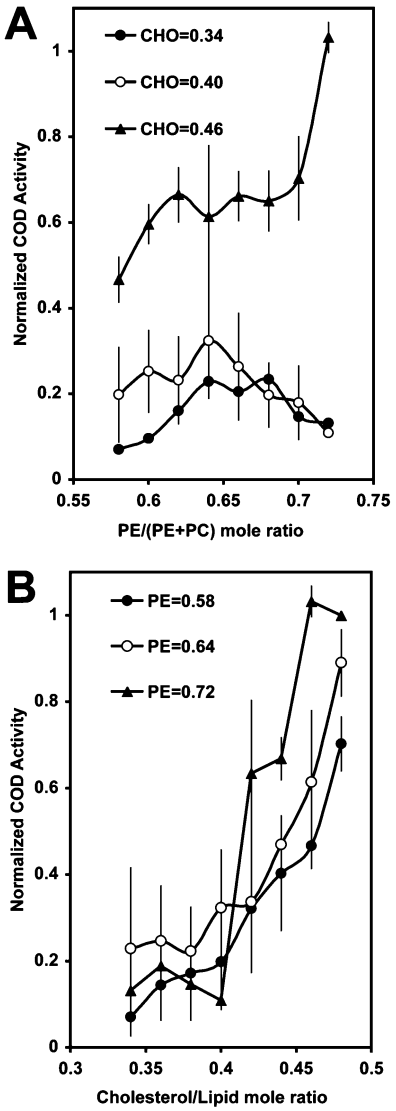

FIGURE 5: Normalized COD activity as a function of PE-to-(PE + PC) or cholesterol-to-lipid mole ratio for POPE/POPC/CHOL liposomes. The normalized COD activity as a function of PE/(PE + PC) mole ratio (A) for a fixed cholesterol-to-lipid mole ratio of 0.34 (●), 0.40 (○), and 0.46 (▲) and as a function of CHOL/Lipid mole ratio (B) for a fixed PE/(PE + PC) mole ratio of 0.58 (●), 0.64 (○) and 0.72 (▲) for POPE/POPC/CHOL liposomes at 37 °C. All COD activity was normalized with respect to the activity at PE/(PE + PC) = 0.72 and CHOL/Lipid = 0.48. The data represent averages of measurements from three parallel and independently prepared liposomes, and the standard errors (bars) are also shown.

peaks of activity at particular X_{PE} values. Prominent peaks were found at $X_{PE} \approx 0.18$, 0.32, 0.50, 0.64, and 0.72 for a fixed X_{CHOL} of 0.33 or 0.40 (Table 1). These X_{PE} values coincide with the critical compositions predicted by the headgroup superlattice model (see Materials and Methods) and, thus, support the idea that the PL headgroups tend to adopt regular, superlattice-like distributions in the ternary POPE/POPC/CHOL bilayers. However, a few observed critical X_{PE} values, that is, 0.40 and 0.58, are not predicted by the current headgroup superlattice model, which was constructed for binary PL bilayers (*23*). These two PE compositions may correspond to another type of superlattice (or other type of membrane structure) involving all three components, that is, POPE, POPC, and cholesterol.

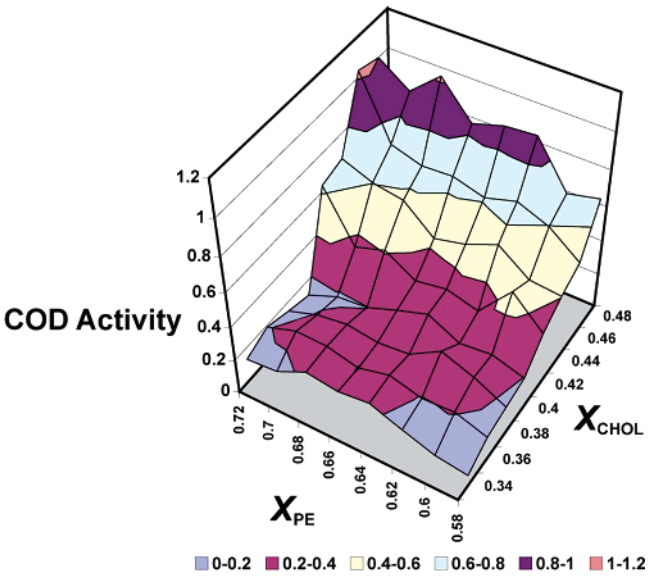

FIGURE 6: Three-dimensional surface plot of normalized COD activity as a function of PE-to-(PE + PC) and cholesterol-to-lipid mole ratio for POPE/POPC/CHOL liposomes. Surface plot of the normalized COD activity as a function of the 2-D lipid composition coordinates, i.e., PE/(PE + PC) and CHOL/Lipid mole ratios, for POPE/POPC/CHOL liposomes at 37 °C is shown. See legend of Figure 5 for other details.

Measurements were performed to examine the dependence of the COD activity with the cholesterol content in binary POPC/CHOL and ternary POPE/POPC/CHOL bilayers. For POPC/CHOL bilayers, a threshold was found at a X_{CHOL} value of 0.4, in agreement with an earlier study carried out with egg PC/CHOL bilayers (*18*). A similar biphasic response was also found for ternary bilayers containing PE (*18*). Interestingly, this critical X_{CHOL} value coincides with the critical X_{CHOL} value of 0.40 predicted for the cholesterol superlattice model (*25*, *35*, *36*). This suggests that the formation of a cholesterol superlattice at the acyl chain level may be associated with the onset of COD activity at that critical region of $X_{CHOL} \approx 0.4$. In addition, our recent probe-dependent and noninvasive Fourier transform IR spectroscopic study on the same POPC/CHOL bilayers also revealed abrupt changes in the physical properties of the bilayer at $X_{CHOL} \approx 0.4$ (*32*), supporting the presence of putative headgroup superlattice domains at that critical cholesterol composition.

When studying composition-dependent phenomena in lipid bilayers, it is important to avoid the demixing of lipid species, which can occur especially with mixtures containing cholesterol (*32*, *60*, *61*). In the present study, binary liposomes prepared by three liposome preparation protocols, that is, membrane extrusion, ethanol injection and RSE, produced comparable results for the onset of COD activity at $X_{CHOL} \approx 0.4$. However, the use of ethanol injection or the extrusion method was not feasible for ternary bilayers with $X_{PE} > 0$ because (i) POPE is insoluble in ethanol and (ii) the use of the extrusion method would require laborious analysis of the lipid concentrations and compositions in each sample. In addition, samples with $X_{CHOL} > 0.35$ were difficult to extrude, had less than 60% recovery, and usually required the multiple exchange of filters with decreasing pore size. For these reasons, the RSE method was used exclusively to prepare POPE/POPC/CHOL liposomes. Previous work

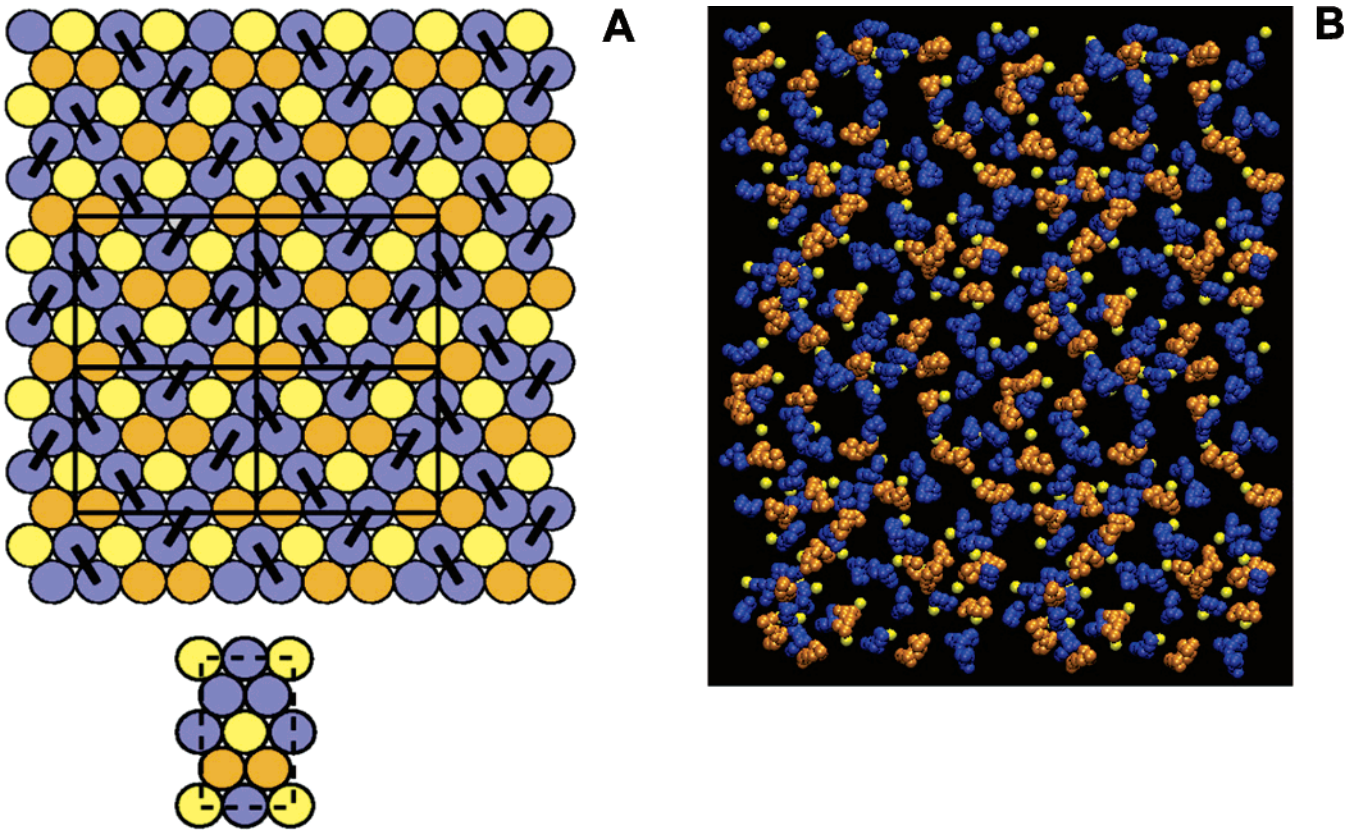

FIGURE 7: Visualization of surface molecular structures of the headgroup and cholesterol superlattices in PE/PC/CHOL bilayers. Space-filling construction: Panel A shows the molecular organization of the PL headgroups. The PE/PC headgroup superlattice is composed of unit cells with center rectangular (CR) symmetry. Here, each phospholipid, host PE (two blue disks connected by a bar representing its two acyl chains), and guest PC (two adjacent orange disks representing its two acyl chains) is identified. PE and PC are shown at a ratio of 2:1, corresponding to $X_{PE} = 0.67$. The solid squares show four representative CR unit cells. The tail group superlattice structure with CR symmetry that matches the headgroup arrangement is also shown. Here, two offset tail group unit cells match each headgroup unit cell (*26*). The unit cell of the superlattice tailgroup is shown by the dashed square. Surface molecular structures of PE/PC/CHOL: Panel B shows the 30 ns MD-simulated molecular organization of polar headgroups, i.e., phosphatidylethanolamine (blue) and phosphatidylcholine (orange) of POPE and POPC, respectively, and the polar 3β hydroxyl group of cholesterol (yellow), constructed by the arrangement of Panel A using GROMACS (*38*). The *x*- and *y*-repeated unit cluster of a basic system of 120 lipid molecules, i.e., one of the two monolayers of the POPE/POPC/CHOL, is shown. For clarity, water molecules are not shown. See Materials and Methods for details.

has shown that this method avoids the demixing of cholesterol (*31*). In addition, the accessible external surface in RSE liposomes is about 33% of the total lipids, which is rather close to the 50% theoretical value of the accessible surface of unilamellar vesicles made from ethanol injection (*31*).

Different methods have been used to measure the cholesterol oxidation activity of COD in lipid bilayers. A direct method is to monitor the absorption of the cholesterol oxidized product, that is, conjugated enone, at 240 nm (*16*, *22*). An indirect method is to monitor selected dye absorption (*34*) or fluorophore fluorescence (*16*) emission at a particular wavelength using a horseradish peroxidase coupled assay, which results in the formation of H_2O_2, a byproduct of cholesterol oxidation. Recently, the fluorescence intensity decay of dehydroergosterol, a fluorescent analogue of cholesterol, has also been used to monitor the COD activity of PC/DHE bilayers (*22*). To avoid membrane damage due to the presence of H_2O_2 in the direct assay, catalase was added to the assay to prevent the peroxidation of the double bonds in the acyl chains (*16*). Similar trends (results not shown) were obtained in the composition dependence of COD activity using the direct method compared with that in the coupled enzyme system.

The action of COD on the membrane surface and the molecular mechanisms of the regulation of COD activity by the physical properties of the bilayers have been studied using various PL/CHOL bilayers. It was suggested that the enzyme interacts directly with the membrane surface, typically through the PL headgroup without significant penetration or perturbation of the membrane (*14*, *15*). After membrane binding, the enzyme undergoes a conformational change and, subsequently, creates a hydrophobic pathway or channel to extract the cholesterol from the bilayer and directs it to the active site of the enzyme (*16*). This mechanism of COD hydrolytic action does not involve the leakage of cholesterol from the membrane due to COD binding (*15*, *19*). Previous work has also shown that the enzyme COD has greater binding affinity for membranes in a solid-order state than those in the fluid state (*16*). In addition, the binding affinity is independent of the cholesterol mole fraction when the membranes are in a fluid state (*16*). Therefore, the peaks or kinks in COD activity versus lipid composition plots are likely to be associated with the abrupt changes in the accessibility or chemical activity of membrane cholesterol.

The accessibility of cholesterol to the enzyme may be associated with the hydration of the membrane surface. Previous studies have indicated that the hydration of the

bilayer surface increases as the lipid molecules become more regularly distributed (*22*, *32*). Other experiments on binary PC/CHOL bilayers further suggested that the increased hydration associated with the superlattice domains results in greater availability of the cholesterol to the enzyme and, hence, enhances the oxidation rate of cholesterol (*22*, *32*). A recent Fourier transform IR spectroscopic study on identical POPE/POPC/CHOL bilayers, as in this present study, also indicated an abrupt increase in the hydration of the lipid phosphate groups at several critical PE compositions (*26*). This further supports the hypothesis that the altered hydration due to superlattice organization at the membrane surface represents one possible modulation mechanism of COD activity by headgroup composition in a ternary lipid bilayer.

The 3-D surface plot of COD activity for the POPE/POPC/CHOL bilayers shown in Figure 6 allows a better visualization of the effects of PE and CHOL on the surface accessibility of cholesterol to COD. The PE-dependent increase in the sharpness of the onset of COD activity at the cholesterol threshold of $X_{CHOL} \approx 0.4$ indicates that cholesterol becomes more accessible to the enzyme with increasing PE content. This could be due to the fact that the smaller head group of PE cannot shield the cholesterol from the aqueous phase as effectively as the bigger and more hydrated headgroup of PC (*60*, *62*). Our molecular simulation result (Figure 7B) indicates that the cholesterol headgroups are reasonably exposed in ternary mixtures with high PE content. However, there may still be appreciable steric hindrance from the large PC headgroups that lowers accessibility to the enzyme. Detailed experimental and molecular simulation studies are still needed to address the issue of cholesterol accessibility on the membrane surface of bilayers of compositions other than PE/PC to surface-acting enzymes.

Besides the putative alterations in membrane surface hydration, other changes could occur at the critical PE compositions. First, it is possible that an increase in membrane lateral order within the headgroup superlattice domains may result in an increase in the reorientation or increased freedom of the PL headgroups so that the cholesterol transfer from the membrane to the hydrophobic channel of COD may be enhanced. This notion of the more disordered PL headgroup at the critical superlattice compositions is supported by a recent FTIR study of the same POPC/POPE/CHOL bilayers (*26*). Second, the cholesterol is well spaced in the superlattice structure, and only one monomer cholesterol is allowed to enter the hydrophobic channel of COD (*12*) for subsequent oxidation. To the hydrophobic cholesterol entrance site of COD, all cholesterol molecules within the superlattice domain appear to have the same local molecular environment, surrounded uniformly by PE and PC. This uniform spacing organization of monomer cholesterol could enhance the ability of COD to target cholesterol on the membrane surface. Third, altered motional freedom of cholesterol in the superlattice domain environment at both headgroup and tail group levels may facilitate its transfer into the hydrophobic pathway of COD.

In conclusion, our results indicate that the model membrane-surface-acting enzyme, bacterial COD, is modulated by the putative headgroup superlattices below the cholesterol threshold of $X_{CHOL} \approx 0.4$. In addition, PE, a PL with a small headgroup, effectively enhances COD activity when the cholesterol content exceeds the above threshold. More detailed molecular dynamics studies of the surface-acting enzyme and multicomponent bilayer surface of different molecular organizations are still needed to examine the interesting lipid domain and peptide interactions on the membrane surface at the molecular level.

REFERENCES

1. Simons, K., and Ehehalt, R. (2002) Cholesterol, lipid rafts, and disease, *J. Clin. Invest. 110*, 597−603.
2. Maxfield, F. R., and Tabas, I. (2005) Role of cholesterol and lipid organization in disease, *Nature 438*, 612−621.
3. Wood, W. G., Schroeder, F., Igbavboa, U., Avdulov, N. A., and Chochina, S. V. (2002) Brain membrane cholesterol domains, aging and amyloid beta-peptides, *Neurobiol. Aging 23*, 685−694.
4. Subasinghe, S., Unabia, S., Barrow, C. J., Mok, S. S., Aguilar, M. I., and Small, D. H. (2003) Cholesterol is necessary both for the toxic effect of Abeta peptides on vascular smooth muscle cells and for Abeta binding to vascular smooth muscle cell membranes, *J. Neurochem. 84*, 471−479.
5. Puglielli, L., Friedlich, A. L., Setchell, K. D., Nagano, S., Opazo, C., Cherny, R. A., Barnham, K. J., Wade, J. D., Melov, S., Kovacs, D. M., and Bush, A. I. (2005) Alzheimer disease beta-amyloid activity mimics cholesterol oxidase, *J. Clin. Invest. 115*, 2556−2563.
6. Mason, R. P., and Jacob, R. F. (2003) Membrane microdomains and vascular biology: emerging role in atherogenesis, *Circulation 107*, 2270−2273.
7. Tulenko, T. N., Sumner, A. E., Chen, M., Huang, Y., Laury-Kleintop, L., and Ferdinand, F. D. (2001) The smooth muscle cell membrane during atherogenesis: a potential target for amlodipine in atheroprotection, *Am. Heart J. 141*, S1−S11.
8. Giddings, K. S., Johnson, A. E., and Tweten, R. K. (2003) Redefining cholesterol's role in the mechanism of the cholesterol-dependent cytolysins, *Proc. Natl. Acad. Sci. U. S. A. 100*, 11315−21130.
9. Navas, J., Gonzalez-Zorn, B., Ladron, N., Garrido, P., and Vazquez-Boland, J. A. (2001) Identification and mutagenesis by allelic exchange of choE, encoding a cholesterol oxidase from the intracellular pathogen Rhodococcus equi, *J. Bacteriol. 183*, 4796−4805.
10. Av-Gay, Y., and Sobouti, R. (2000) Cholesterol is accumulated by mycobacteria but its degradation is limited to non-pathogenic fast-growing mycobacteria, *Can. J. Microbiol. 46*, 826−831.
11. Sampson, N. S., and Vrielink, A. (2003) Cholesterol oxidases: a study of nature's approach to protein design, *Acc. Chem. Res. 36*, 713−722.
12. Lario, P. I., Sampson, N., and Vrielink, A. (2003) Sub-atomic resolution crystal structure of cholesterol oxidase: what atomic resolution crystallography reveals about enzyme mechanism and the role of the FAD cofactor in redox activity, *J. Mol. Biol. 326*, 1635−1650.
13. Sampson, N. S., Mrksich, M., and Bertozzi, C. R. (2001) Surface molecular recognition, *Proc. Natl. Acad. Sci. U. S. A. 98*, 12870−12871.
14. Chen, X., Wolfgang, D. E., and Sampson, N. S. (2000) Use of the parallax-quench method to determine the position of the active-site loop of cholesterol oxidase in lipid bilayers, *Biochemistry 39*, 13383−13389.
15. Sampson, N. S., Kass, I. J., and Ghoshroy, K. B. (1998) Assessment of the role of an omega loop of cholesterol oxidase: a truncated loop mutant has altered substrate specificity, *Biochemistry 37*, 5770−5778.
16. Ahn, K. W., and Sampson, N. S. (2004) Cholesterol oxidase senses subtle changes in lipid bilayer structure, *Biochemistry 43*, 827−836.
17. De Martinez, S. G., and Green, C. (1979) The action of cholesterol oxidase on cholesterol in vesicles and micelles [proceedings], *Biochem. Soc. Trans. 7*, 978−979.
18. Pal, R., Barenholz, Y., and Wagner, R. R. (1980) Effect of cholesterol concentration on organization of viral and vesicle membranes. Probed by accessibility to cholesterol oxidase, *J Biol. Chem. 255*, 5802−5806.
19. Ghoshroy, K. B., Zhu, W., and Sampson, N. S. (1997) Investigation of membrane disruption in the reaction catalyzed by cholesterol oxidase, *Biochemistry 36*, 6133−6140.

20. Mattjus, P., and Slotte, J. P. (1996) Does cholesterol discriminate between sphingomyelin and phosphatidylcholine in mixed monolayers containing both phospholipids? *Chem. Phys. Lipids 81*, 69−80.
21. Lange, Y., Ye, J., and Steck, T. L. (2004) How cholesterol homeostasis is regulated by plasma membrane cholesterol in excess of phospholipids, *Proc. Natl. Acad. Sci. U. S. A. 101*, 11664−11667.
22. Wang, M. M., Olsher, M., Sugar, I. P., and Chong, P. L. (2004) Cholesterol superlattice modulates the activity of cholesterol oxidase in lipid membranes, *Biochemistry 43*, 2159−21566.
23. Cheng, K. H., Ruonala, M., Virtanen, J., and Somerharju, P. (1997) Evidence for superlattice arrangements in fluid phosphatidylcholine/phosphatidylethanolamine bilayers, *Biophys. J. 73*, 1967−1976.
24. Virtanen, J. A., Cheng, K. H., and Somerharju, P. (1998) Phospholipid composition of the mammalian red cell membrane can be rationalized by a superlattice model, *Proc. Natl. Acad. Sci. U.S.A. 95*, 4964−4969.
25. Somerharju, P., Virtanen, J. A., and Cheng, K. H. (1999) Lateral organisation of membrane lipids. The superlattice view, *Biochim. Biophys. Acta 1440*, 32−48.
26. Cannon, B., Lewis, A., Metze, J., Thiagarajan, V., Vaughn, M. W., Somerharju, P., Virtanen, J., Huang, J., and Cheng, K. H. (2006) Cholesterol supports headgroup superlattice domain formation in fluid phospholipid/cholesterol bilayers, *J. Phys. Chem. B 110*, 6339−6350.
27. Cheng, K. H., Virtanen, J., and Somerharju, P. (1999) Fluorescence studies of dehydroergosterol in phosphatidylethanolamine/phosphatidylcholine bilayers, *Biophys. J. 77*, 3108−3119.
28. Kingsley, P. B., and Feigenson, G. W. (1979) The synthesis of a perdeuterated phospholipid: 1, 2-dimyristoyl-sn-glycero-3-phosphocholine-d72, *Chem. Phys. Lipids 24*, 135−147.
29. Hope, M. J., Bally, M. B., Webb, G., and Cullis, P. R. (1985) Production of large unilamellar vesicles by rapid extrusion procedure. Characterization of size distribution, trapped volume and ability to maintain membrane potential, *Biochim. Biophys. Acta 812*, 55−65.
30. Batzri, S., and Korn, E. D. (1973) Single bilayer liposomes prepared without sonication, *Biochim. Biophys. Acta 298*, 1015−1019.
31. Buboltz, J. T., and Feigenson, G. W. (1999) A novel strategy for the preparation of liposomes: rapid solvent exchange, *Biochim. Biophys. Acta 1417*, 232−245.
32. Cannon, B., Heath, G., Huang, J., Somerharju, P., Virtanen, J. A., and Cheng, K. H. (2003) Time-resolved fluorescence and fourier transform infrared spectroscopic investigations of lateral packing defects and superlattice domains in compositionally uniform cholesterol/phosphatidylcholine bilayers, *Biophys. J. 84*, 3777−3791.
33. Parker, A., Miles, K., Cheng, K. H., and Huang, J. (2004) Lateral distribution of cholesterol in dioleoylphosphatidylcholine lipid bilayers: cholesterol-phospholipid interactions at high cholesterol limit, *Biophys. J. 86*, 1532−1544.
34. Allain, C. C., Poon, L. S., Chan, C. S., Richmond, W., and Fu, P. C. (1974) Enzymatic determination of total serum cholesterol, *Clin. Chem. 20*, 470−475.
35. Chong, P. L., and Sugar, I. P. (2002) Fluorescence studies of lipid regular distribution in membranes, *Chem. Phys. Lipids 116*, 153−175.
36. Chong, P. L.-G., and Olsher, M. (2004) Fluorescence studies of the existence and functional importance of regular distribution in liposomal membranes, *Soft Materials 2*, 85−108.
37. Cannon, B., Hermansson, M., Gyorke, S., Somerharju, P., Virtanen, J. A., and Cheng, K. H. (2003) Regulation of calcium channel activity by lipid domain formation in planar lipid bilayers, *Biophys. J. 85*, 933−942.
38. *GROMACS*. Gromacs molecular topologies, http://www.gromacs.org/topologies/molecules.php (accessed May 2006).
39. Berendsen, H. D., van der Spoel, D., and van Drunen, R. (1995) GROMACS: A message-passing parallel molecular dynamics implementation, *Comput. Phys. Commun. 91*, 43−56.
40. Lindahl, E., Hess, B., and van der Spoel, D. (2001) GROMACS 3.0: A package for molecular simulation and trajectory analysis, *J. Mol. Model. 7*, 306−317.
41. Tieleman, D. P., Sansom, M. S., and Berendsen, H. J. (1999) Alamethicin helices in a bilayer and in solution: molecular dynamics simulations, *Biophys. J. 76*, 40−49.
42. Tieleman, D. P. (2005) http://moose.bio.ucalgary.ca/index.php?page=Downloads.
43. Tieleman, D. P., and Berendsen, H. J. (1998) A molecular dynamics study of the pores formed by Escherichia coli OmpF porin in a fully hydrated palmitoyloleoylphosphatidylcholine bilayer, *Biophys. J. 74*, 2786−2801.
44. Holtje, M., Forster, T., Brandt, B., Engels, T., von Rybinski, W., and Holtje, H. D. (2001) Molecular dynamics simulations of stratum corneum lipid models: fatty acids and cholesterol, *Biochim. Biophys. Acta 1511*, 156−167.
45. *RCSB. Protein Data Bank, Protein Data Bank Contents Guide: Atomic Coordinate Entry Format Description*, v2.2, http://www.rcsb.org/pdb/file_formats/pdb/pdbguide2.2/guide2.2_frame (accessed May 2006).
46. Berendsen, H. J. C., Postma, J. P. M., van Gunsteren, W. F., and Hermans, J. (1981) Interaction Models for Water in Relation to Protein Hydration, in *Intermolecular Forces* (Pullman, B., Ed.) pp 331−342, Reidel, Dordrecht, The Netherlands.
47. Berendsen, H. J. C., Postma, J. P. M., van Gunsteren, W. F., DiNola, A., and Haak, J. R. (1984) Molecular dynamics with coupling to an external bath, *J. Chem. Phys. 81*, 3684−3690.
48. Berger, O., Edholm, O., and Jahnig, F. (1997) Molecular dynamics simulations of a fluid bilayer of dipalmitoylphosphatidylcholine at full hydration, constant pressure, and constant temperature, *Biophys. J. 72*, 2002−2013.
49. Darden, T., York, D., and Pedersen, L. (1993) Particle mesh Ewald: An N·log(N) method for Ewald sums in large systems, *J. Chem. Phys. 98*, 10089−10092.
50. Essmann, U., Perera, L., Berkowitz, M. L., Darden, T., Lee, H., and Pedersen, L. (1995) A smooth particle mesh Ewald method, *J. Chem. Phys. 103*, 8577−8593.
51. Hess, B., Bekke, H., Berendsen, H. J. C., and Fraaije, J. G. E. M. (1997) LINCS: a linear constraint solver for molecular simulations, *J. Comput. Chem. 13*, 952−962.
52. Hockney, R. W., Geol, S. P. J., and Eastwood, J. W. (1974) Quiet high-resolution computer models of a plasma, *J. Comput. Phys. 98*, 10089−10092.
53. Humphrey, W., Dalke, A., and Schulten, K. (1996) VMD: Visual molecular dynamics, *J. Mol. Graphics 14*, 33−38.
54. Whittaker, E. T., and Robinson, G. (1967) *Graduation, or the Smoothing of Data*, 4th ed., Dover, New York.
55. Anderson, R. G., and Jacobson, K. (2002) A role for lipid shells in targeting proteins to caveolae, rafts, and other lipid domains, *Science 296*, 1821−1825.
56. Simons, K., and Ikonen, E. (1997) Functional rafts in cell membranes, *Nature 387*, 569−572.
57. Simons, K., and van Meer, G. (1988) Lipid sorting in epithelial cells, *Biochemistry 27*, 6197−6202.
58. Simons, K., and Vaz, W. L. (2004) Model systems, lipid rafts, and cell membranes, *Annu. Rev. Biophys. Biomol. Struct. 33*, 269−295.
59. Liu, F., and Chong, P. L. (1999) Evidence for a regulatory role of cholesterol superlattices in the hydrolytic activity of secretory phospholipase A2 in lipid membranes, *Biochemistry 38*, 3867−3873.
60. Huang, J., Buboltz, J. T., and Feigenson, G. W. (1999) Maximum solubility of cholesterol in phosphatidylcholine and phosphatidylethanolamine bilayers, *Biochim. Biophys. Acta 1417*, 89−100.
61. Huang, J. (2002) Exploration of molecular interactions in cholesterol superlattices: effect of multibody interactions, *Biophys. J. 83*, 1014−1025.
62. Huang, J., and Feigenson, G. W. (1999) A microscopic interaction model of maximum solubility of cholesterol in lipid bilayers, *Biophys. J. 76*, 2142−2157.

BI060937Y